SCIENTIFIC REPORTS

OPEN

SUBJECT AREAS:
NANOPARTICLES
BATTERIES

Received
31 October 2013

Accepted
27 November 2013

Published
16 December 2013

Correspondence and requests for materials should be addressed to Y.W. (yongwang@shu.edu.cn)

Large and fast reversible Li-ion storages in Fe_2O_3-graphene sheet-on-sheet sandwich-like nanocomposites

Jin Kan & Yong Wang

Department of Chemical Engineering, School of Environmental and Chemical Engineering, Shanghai University, Shangda Road 99, Shanghai, P. R. China, 200444.

Fe_2O_3 nanosheets and nanoparticles are grown on graphene by simply varying reaction solvents in a facile solvothermal/hydrothermal preparation. Fe_2O_3 nanosheets are uniformly dispersed among graphene nanosheets, forming a unique sheet-on-sheet nanostructure. Due to the structure affinity between two types of two dimensional nanostructures, graphene nanosheets are separated better by Fe_2O_3 nanosheets compared to nanoparticles and their agglomeration is largely prevented. A large surface area of 173.9 $m^2 g^{-1}$ is observed for Fe_2O_3-graphene sheet-on-sheet composite, which is more than two times as large as that of Fe_2O_3-graphene particle-on-sheet composite (81.5 $m^2 g^{-1}$). The sheet-on-sheet composite is found to be better suitable as an anode for Li-ion battery. A high reversible capacity of 662.4 mAh g^{-1} can be observed after 100 cycles at 1000 mA g^{-1}. The substantially improved cycling performance is ascribed to the unique structure affinity between Fe_2O_3 nanosheets and graphene nanosheets, thus offering complementary property improvement.

Lithium-ion battery is considered as one of the best power sources to maximize the efficiency of energy use. Graphite has been widely used as an anode material for commercial Li-ion batteries with a low theoretical specific capacity (372 mAh g^{-1}). In recent years, metal oxides such as Fe_2O_3, NiO, CuO and SnO_2 have been the focus of anode materials for Li-ion battery due to the increasing demand for high energy storage[1–4]. These metal oxides electrodes have shown much higher Li-ion storage capacities than that of commercial graphite anodes[1]. Among these oxides, Fe_2O_3 is a promising anode material because of low cost, simple manufacturing process, wide range of sources, environmental friendliness and the most important factor, a large theoretical specific capacity (1007 mAh g^{-1})[5–15]. However, their cycling performances are not satisfactory because partial pulverization and electrode cracking may take place upon repetitive cycling reactions between Fe_2O_3 and Li ions[7–15].

Various carbon materials have been attempted to be composited with high-capacity metal oxides to improve their electrical contact and structure stability during cycling[16–21]. Graphene nanosheet (GNS), a flat monolayer of sp^2-bonded carbon atoms, has been one of the most popular research hotspots. Its high electrical conductivity, large specific surface area and highly flexible and stable structure are also desirable for Li-ion storage applications[22–24]. Recently, various metal oxides-GNS nanocomposites have been reported as promising anode materials for Li-ion batteries with substantially improved electrochemical performances[25–46]. It is known that the electrochemical properties of nanostructured anode materials are dependent on their morphology and size. Therefore Fe_2O_3-based anode materials have been synthesized with a variety of Fe_2O_3 morphologies such as nanoparticle[7–10,31–42], nanotube[11], nanoflake[12], nanorod[9,34], nanodendrite[13], nanodisk[15,43,44], nanorice[29], and nanospindle[30].

In this work, a new Fe_2O_3-graphene structure, namely sheet-on-sheet nanostructure, was prepared by a solvothermal method. Fe_2O_3 nanoparticles were also prepared on graphene nanosheets by varying the reaction solvent. The Fe_2O_3-graphene sheet-on-sheet nanostructure was fabricated as an anode for Li-ion batteries. The specific capacities and cycling performances of Fe_2O_3-graphene sheet-on-sheet composite were found to be much better than pristine Fe_2O_3 nanosheets and Fe_2O_3-graphene particle-on-sheet composite, especially at high rates. A high capacity of 662.4 mAh g^{-1} for the sheet-on-sheet composite could be retained after 100 cycles at 1 C.

Results

Characterizations of Fe_2O_3-graphene composites. Fig. 1a shows the crystal phase of Fe_2O_3 nanoparticle, Fe_2O_3 nanosheet, Fe_2O_3-graphene particle-on-sheet and Fe_2O_3-graphene sheet-on-sheet. All diffraction peaks in these

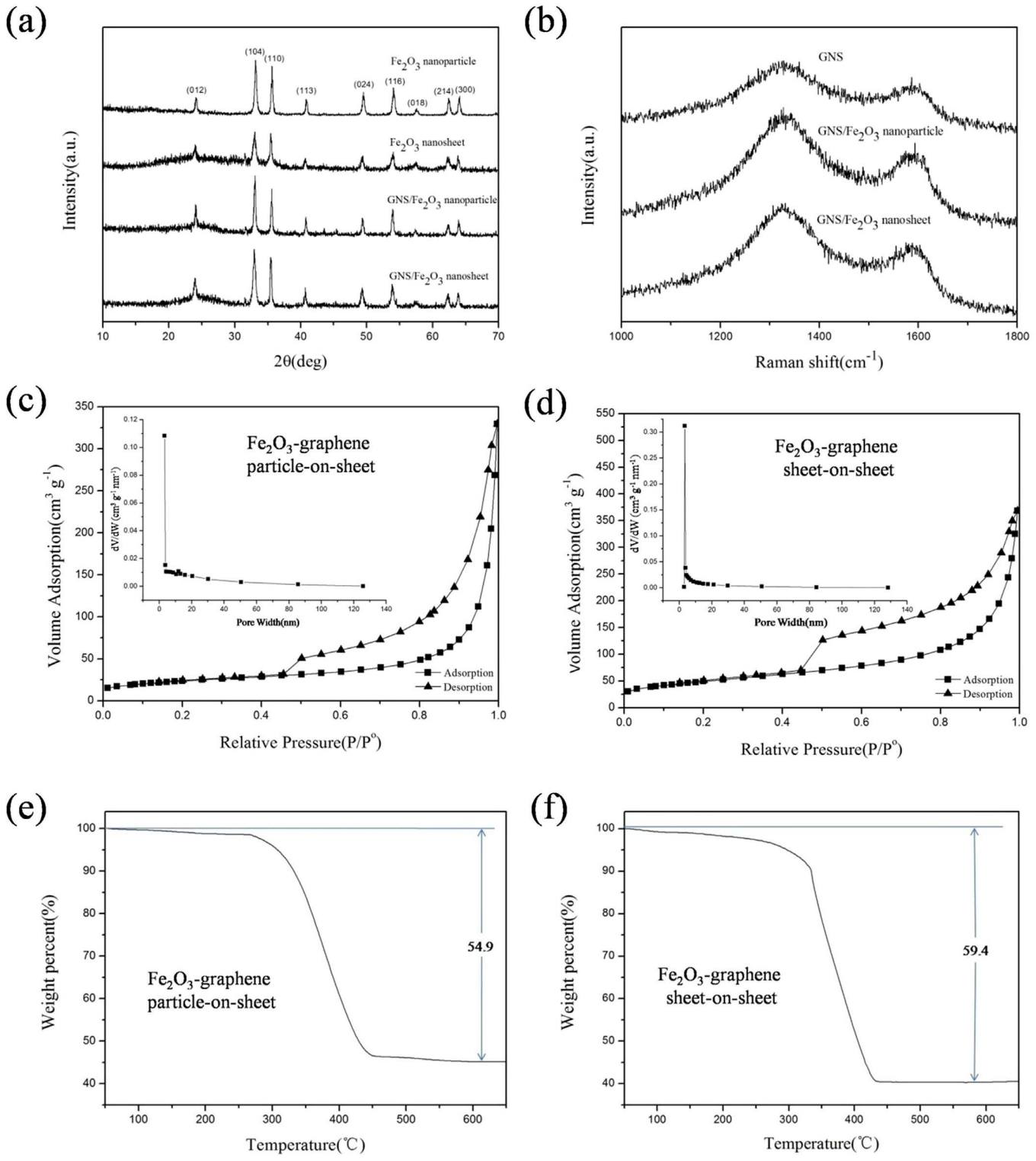

Figure 1 | Structural analysis of Fe_2O_3-based products. (a) Powder X-ray diffraction (XRD) patterns of various Fe_2O_3-based products, (b) Raman spectrum. Nitrogen sorption isotherms of (c) Fe_2O_3-graphene particle-on-sheet composite, and (d) Fe_2O_3-graphene sheet-on-sheet composite, TGA curves of (e) Fe_2O_3-graphene particle-on-sheet and (f) Fe_2O_3-graphene sheet-on-sheet.

samples can be assigned well to the standard Fe_2O_3 (PDF 33-0664). There is no clear observation of the (002) diffraction peak of graphene, because the (012) diffraction peak of hematite is strong, which can shadow the (002) peak at the similar 2θ[23,24]. Fig. 1b shows the Raman spectra of graphene nanosheet (GNS), Fe_2O_3-graphene particle-on-sheet and Fe_2O_3-graphene sheet-on-sheet. All three samples display similar two bands at ~1320 and 1580 cm^{-1}, which correspond to the disordered (D) band and graphitic (G) band of carbon materials respectively[47]. The intensity ratios of the D to G band (I_D: I_G) are calculated to be 1.34 and 1.36 for Fe_2O_3-graphene particle-on-sheet and sheet-on-sheet composite, respectively, which are both larger than that of GNS (1.18). This enhancement of the disordered carbon content should be ascribed to the partial insertion of Fe_2O_3 nanoparticles or nanosheets into

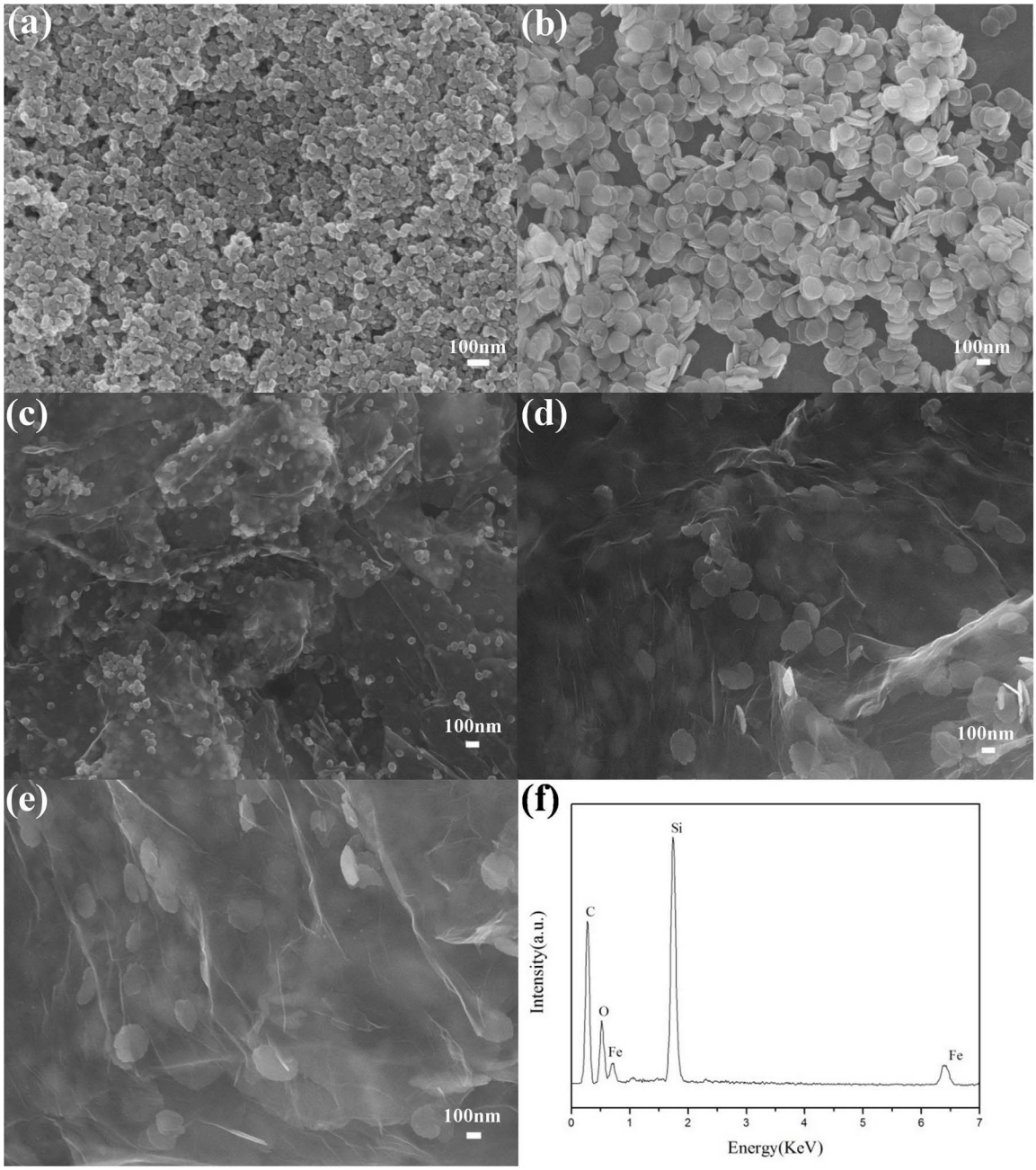

Figure 2 | The morphological analysis of Fe_2O_3-based products by SEM. SEM images of (a) Fe_2O_3 nanoparticle, (b) Fe_2O_3 nanosheet, (c) Fe_2O_3-graphene particle-on-sheet composite, (d, e) Fe_2O_3-graphene sheet-on-sheet composite, and (f) EDS spectra of Fe_2O_3-graphene sheet-on-sheet composite. The Si comes from the substrate for dispersion of the sample.

graphene layer, which is in accordance with previous reports about graphene-based nanocomposites[25,26].

To explore the porous structure and specific surface area of Fe_2O_3-graphene sheet-on-sheet and particle-on-sheet composites, nitrogen sorption investigations have been carried out. The porous attribute of these nanocomposites are shown in Fig. 1c and 1d. Both adsorption and desorption curves exhibit an IUPAC IV type curve characteristic, which indicate that there are many mesopores in two Fe_2O_3-graphene composites. The surface area of Fe_2O_3-graphene sheet-on-sheet is determined to be 173.9 $m^2\ g^{-1}$ by fitting the isotherms to the BET model. This value is substantially higher than that of Fe_2O_3-graphene particle-on-sheet (81.5 $m^2\ g^{-1}$), indicating that graphene nanosheets are separated better in the Fe_2O_3-graphene sheet-on-sheet composite compared to particle-on-sheet composite. This is because nanosheet has a better structure suitability with graphene nanosheets due to their similar two dimensional nanostructures. Therefore there are more contact area between GNS and Fe_2O_3 nanosheet compared to that of the particle-on-sheet composite, which can effectively prevent the reassembly of GNS to graphite platelets. Moreover, nanosheets are more stable than nanoparticles because their sizes are larger than the particle sizes of Fe_2O_3 nanoparticles. In comparison, nanosized Fe_2O_3 particles may be easily agglomerated. The pore size distribution curves of Fe_2O_3-graphene sheet-on-sheet and Fe_2O_3-graphene particle-on-sheet are shown in the inset of Fig. 1c and 1d respectively. Based on the BJH calculation, the sheet-on-sheet composite displays a sharp distribution peak centered at ~3.4 nm, which is similar to that of particle-on-sheet composite (~3.3 nm). These similar pore size distributions indicate that the observed mesopores are mainly from graphene materials in two Fe_2O_3-graphene composites. According to thermal gravimetric

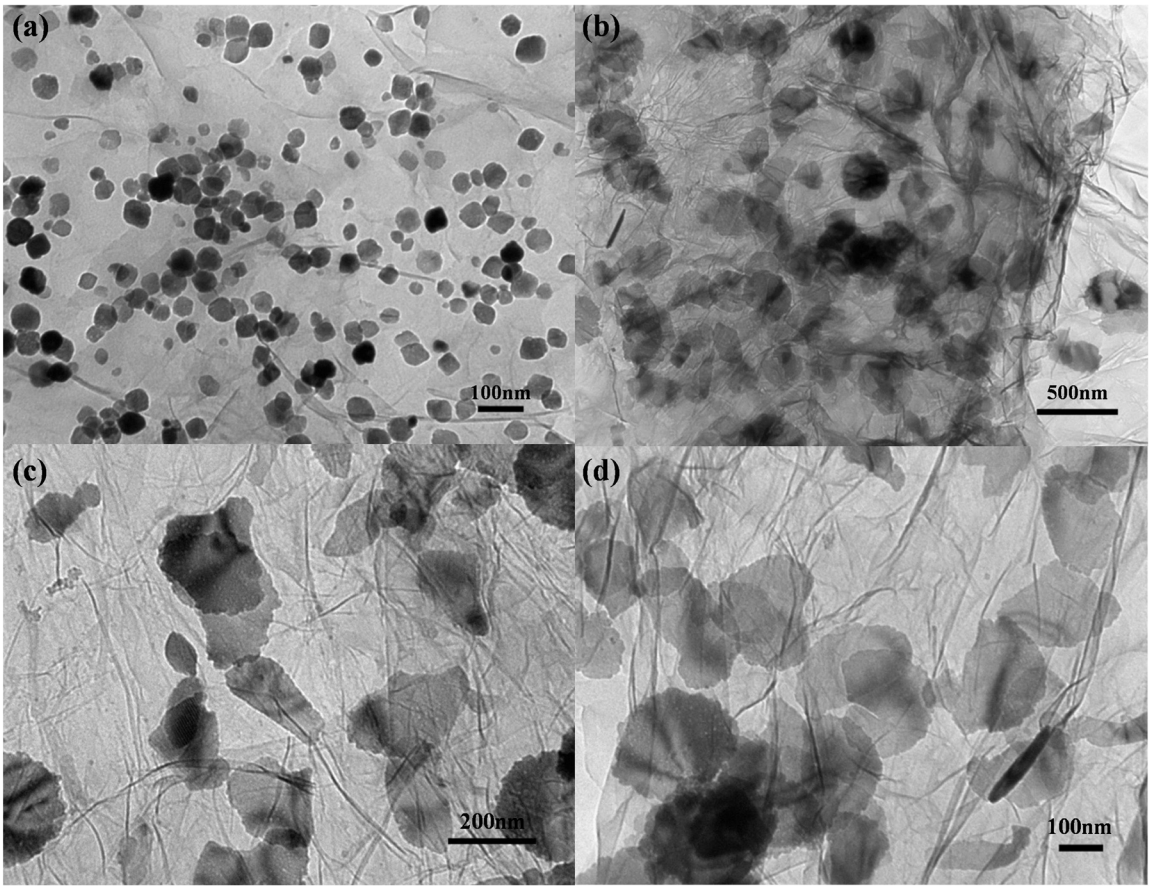

Figure 3 | The morphological analysis of Fe_2O_3-graphene nanocomposites by TEM. TEM images of (a) Fe_2O_3-graphene particle-on-sheet composite, and (b–d) Fe_2O_3-graphene sheet-on-sheet composite with stepwise increased magnifications.

analysis in air as shown in Fig. 1e–f, the weight percentages of graphene were estimated to be 59.4 wt% for Fe_2O_3-graphene sheet-on-sheet and 54.9 wt% for Fe_2O_3-graphene particle-on-sheet. These values are both slightly less than the theoretical value (66.7 wt%), which is calculated based on the experimental conditions.

Fig. 2a–e show SEM images of various Fe_2O_3-based products. A large number of pristine Fe_2O_3 nanoparticles are shown in Fig. 2a. Their particle sizes are ~30–50 nm, which is substantially smaller than that of pristine Fe_2O_3 nanosheets (~100–250 nm in size) as shown in Fig. 2b. In the presence of graphene, Fe_2O_3-graphene particle-on-sheet and sheet-on-sheet composites both have curled paper-like structure (Fig. 2c and 2d–e). It can be shown that Fe_2O_3 nanoparticles and nanosheets are uniformly distributed on graphene nanosheets. Fig. 2e shows clearly that Fe_2O_3 nanosheets are wrapped by graphene nanosheets, and therefore on the other hand, graphene nanosheets are also separated by Fe_2O_3 nanosheets. Notably, compared to Fe_2O_3-graphene sheet-on-sheet, a similar method expect for using deionized water as solvent to replace isopropanol was used to obtain pristine Fe_2O_3 nanoparticles. Fig. 2f shows the energy dispersive energy dispersive spectroscopy (EDS) of Fe_2O_3-graphene sheet-on-sheet composite. A few elements such as C, O, and Fe are present in the composite. The Si element is observed because it was used as a substrate to disperse SEM sample, thus removing the carbon effect from the common carbon support. The carbon contents in the sheet-on-sheet and particle-on-sheet were determined to be 59.7 wt% and 57.9 wt%, which are slightly different from the results indicated from TGA analysis. It is believed that the latter should be more accurate than the EDS results for the determination of materials composition. The particle-on-sheet and sheet-on-sheet nanostructures can be further confirmed by TEM images of Fig. 3a and Fig. 3b–d, respectively. These Fe_2O_3 nanoparticles and nanosheets are uniformly distributed on graphene nanosheets. There is no observation of Fe_2O_3 materials outside the graphene support even after strong sonication in ethanol used for TEM measurement. It should be ascribed to the binding effect of graphene, which can immobilize Fe_2O_3 materials and prevent their movement and agglomeration. Notably, it is clear from TEM images with higher magnifications in Fig. 3c–d that the obtained Fe_2O_3 nanosheets exhibit irregular sheet-like structure with the size of ~100–250 nm.

Exploration of the effect of experimental conditions on Fe_2O_3 morphologies. Fig. 4 shows SEM images of the obtained Fe_2O_3 products by varying the reaction solvent. A large number of thick platelets were obtained by using 10 mL ethanol with 0.07 mL water (Fig. 4a). If 10 mL propanol with 0.07 mL water was used as the solvent, the obtained product exhibited sheet-like structure with larger particle sizes of several hundred nanometers to a few micrometers (Fig. 4b). As reported previously, a trace amount of water can facilitate the crystallization of Fe_2O_3[6]. Therefore various amounts of water were also explored in the preparation. Fig. 4c shows Fe_2O_3 platelets with a smaller size of ~100 nm prepared from 10 mL isopropanol with increased amount of water (0.7 mL). In comparison, agglomerated Fe_2O_3 sheets and platelets were obtained by using 10 mL isopropanol in the absence of water (Fig. 4d). Fig. 5 show SEM images of Fe_2O_3-graphene composites grown from 10 mL propanol (Fig. 5a–b) and the mixed solvent of 10 mL propanol and 0.07 mL water (Fig. 5c–d). Although several Fe_2O_3 sheets can be shown in Fig. 5a and 5c, some nanoparticle products were also observed in Fig. 5b and 5d with higher magnifications. Compared to these benchmarked products by varying reaction solvents, it is

clear that the main products of Fe_2O_3 nanoparticles and nanosheets (as shown in Fig. 2) have more uniform particle size and morphology control. There is also less agglomeration of Fe_2O_3 materials in the corresponding composites. Based on the above observations, it is believed that the mixed solvent of water and isopropyl is a very important factor for the synthesis of sheet-like Fe_2O_3. The organic solution may offer a suitable reaction environment for the growth of sheet-like crystal. The growth process of Fe_2O_3-graphene sheet-on-sheet or particle-on-sheet composites is illustrated in Fig. 5e. Fe_2O_3 nanosheets were obtained in the organic solvent with a trace amount of water, however nanoparticles were formed in a pure aqueous solvent. These Fe_2O_3 nanosheets or nanoparticles were formed among graphene nanosheets, forming a sandwiched sheet-on-sheet or particle-on-sheet nanostructure, which can separate graphene nanosheets against their reassembly. Because Fe_2O_3 nanosheet structure is basically also two dimensional structures similar to graphene nanosheet, therefore it has a large contact area with graphene and better structure affinity. It is believed that Fe_2O_3 nanosheet is a better spacing material compared to Fe_2O_3 nanoparticles, which can be confirmed by higher surface area in sheet-on-sheet composite compared to particle-on-sheet composite (Fig. 1c–d).

Electrochemical properties of Fe_2O_3-graphene composites. To explore the Li-ion storage properties of Fe_2O_3-graphene composites, two Fe_2O_3-graphene composites, carbon black, and polyvinyl difluoride (PVDF) were mixed at the weight ratio of 8 : 1 : 1 as working electrodes. The CV curves of Fe_2O_3-graphene sheet-on-sheet and particle-on-sheet electrodes were performed at a scan rate of 0.1 mV s^{-1} as shown in Fig. 6a. There are two cathodic peaks at ~1.56 V and ~0.68 V for the sheet-on-sheet composite, which can be attributed to the stepwise reduction of Fe^{3+} to Fe^0 and the formation of solid electrolyte interface (SEI) film around the electrode[29,30]. Meanwhile, two anodic peaks at ~1.90 V and ~2.35 V are observed, corresponding to the stepwise oxidation process of Fe^0 to Fe^{2+} and Fe^{2+} to Fe^{3+}, respectively[34,35]. Compared to the sheet-on-sheet composite, the particle-on-sheet composite displays two cathodic peaks and anodic peaks at similar positions with substantially weaker intensity. It is indicated that the sheet-on-sheet composite has a better electrochemical activity due to larger surface area and shorter diffusion route for lithium insertion and extraction reactions. The overall reversible electrochemical reactions process can be described by the following equation[32].

$$Fe_2O_3 + 6Li^+ + 6e^- \Leftrightarrow 2Fe + 3Li_2O$$

Fig. 6b shows the initial discharge (lithium insertion) and charge (lithium extraction) voltage profiles of various anodes at 0.1 C (1 C = 1000 mA g^{-1}). The Fe_2O_3-graphene sheet-on-sheet, Fe_2O_3-graphene particle-on-sheet, Fe_2O_3 nanosheet, Fe_2O_3 nanoparticle and bare graphene exhibited initial discharge capacities of 1652.8, 1421.7, 1140.8, 1279.3, 1413.3 mAh g^{-1} and charge capacities of 1074.9, 890.4, 812.2, 901.6, 863.4 mAh g^{-1} respectively. A Coulombic efficiency of 65% can be calculated for the Fe_2O_3-graphene sheet-on-sheet, which should be largely due to the irreversible capacity loss occurred in the formation of solid electrolyte interface (SEI) film. Notably, the charge capacity (1074.9 mAh g^{-1}) of Fe_2O_3-graphene sheet-on-sheet composite is slightly larger than the theoretical capacity (1007 mAh g^{-1}) of Fe_2O_3. This may be attributed to additional storage of Li-ions in the defects or micro-pores of the sheet-on-sheet composite induced by partial insertion of Fe_2O_3 into graphene. A more disordered carbon structure was observed in Fe_2O_3-graphene

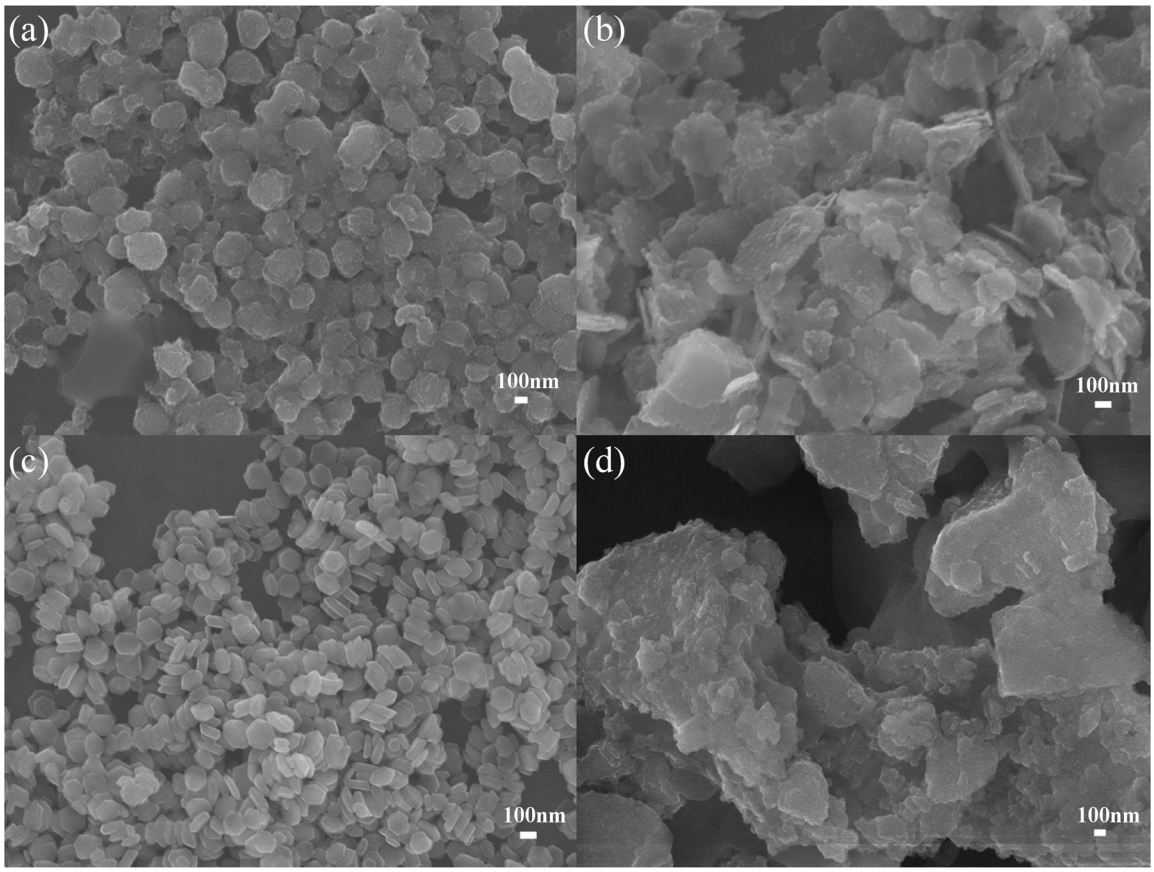

Figure 4 | The morphological analysis of Fe_2O_3 products grown from the different solvent by SEM. (a) 10 mL ethanol with 0.07 mL water, (b) 10 mL propanol with 0.07 mL water, (c) 10 mL isopropanol with 0.7 mL water, and (d) 10 mL isopropanol in the absence of water.

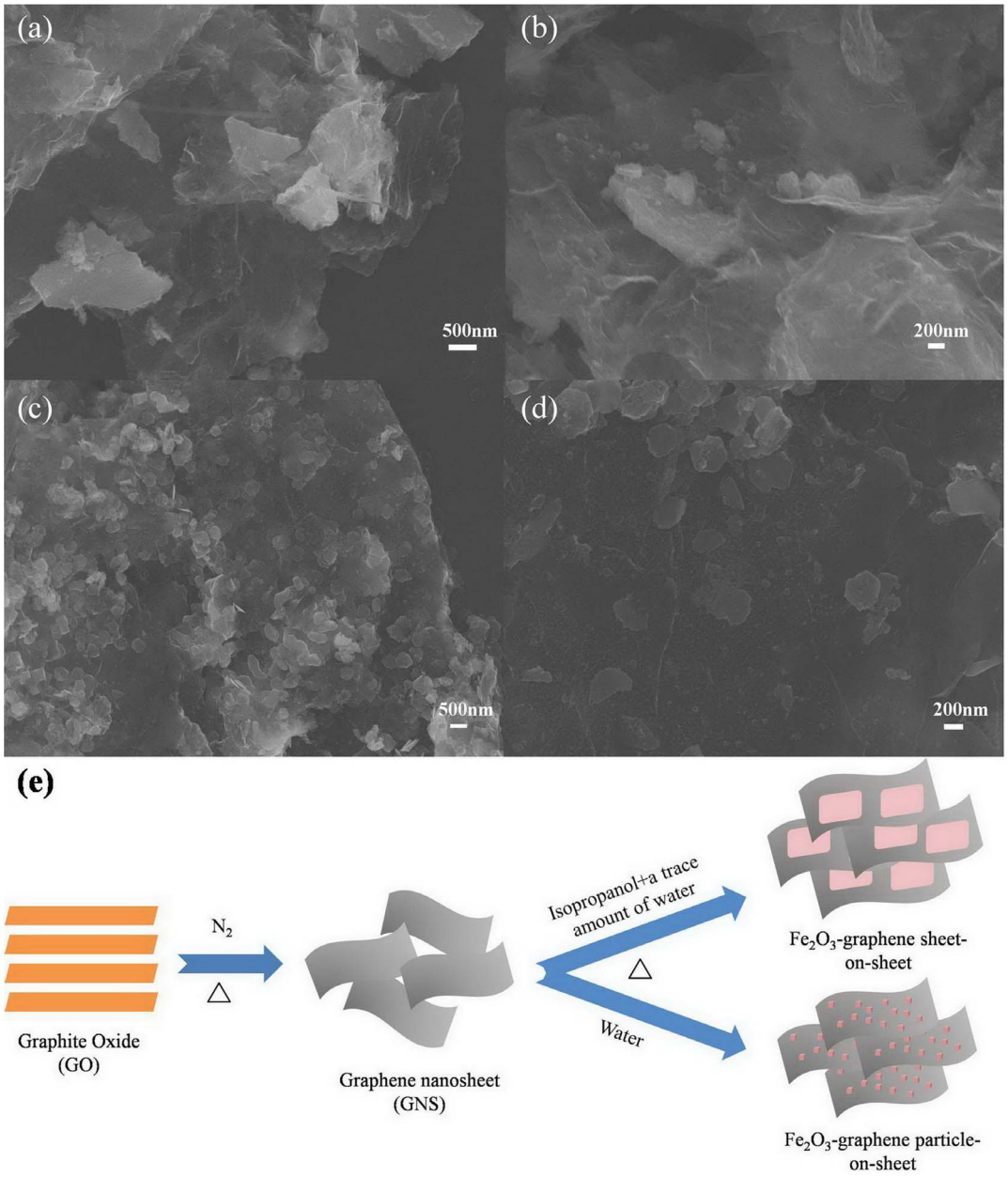

Figure 5 | The morphological analysis of Fe_2O_3-graphene nanocomposites grown from the different solvent by SEM and Schematic illustration. (a, b) 10 mL propanol, and (c, d) 10 mL propanol with 0.07 mL water, (e) Schematic illustration of the growth process of Fe_2O_3-graphene sheet-on-sheet and particle-on-sheet composites.

sheet-on-sheet composite as confirmed by Raman results in Fig. 1b. Compared to the particle-on-sheet composite, the sheet-on-sheet composite also has more active sites for lithium ion storage due to its larger BET surface area. Two voltage plateaus (~1.51 and 0.76 V) are observed in the discharge curve, which can be ascribed to the Li^+ insertion into Fe_2O_3 anode and the formation of SEI film. There are also two voltage plateaus (~1.82 and ~2.27 V) in the charge curve, corresponding to the stepwise oxidation of Fe^0 to Fe^{3+}[34,35]. These observations agree with the CV results as shown in Fig. 6a.

Fig. 6c and 6d compare the cycling performances of the Fe_2O_3-graphene sheet-on-sheet, Fe_2O_3-graphene particle-on-sheet, Fe_2O_3 nanosheet, Fe_2O_3 nanoparticle and bare graphene at a constant small current rate of 0.1 C. Pristine Fe_2O_3 nanoparticle displayed a fast capacity fading from first-cycle 901.6 mAh g^{-1} to 367.1 mAh g^{-1} after 50 cycles. In comparison, Fe_2O_3 nanosheet showed a lower initial charge capacity than Fe_2O_3 nanoparticle, but much better cycling performance in 50 cycles. A higher charge capacity of 466.3 mAh g^{-1} could be observed after 50 cycles. Bare graphene exhibited similar capacity fading to that of Fe_2O_3 nanosheet and a charge capacity of 468.5 mAh g^{-1} was observed after 50 cycles. The cycling stabilities of two Fe_2O_3-graphene composites are both better than pristine Fe_2O_3 nanoparticles or nanosheets. It should be ascribed to the positive contribution from the graphene nanosheet support. It can be found that graphene play a positive role for improving the performance of Fe_2O_3 as anodes for Li ion batteries. Graphene can not only provide a large specific surface area for the insertion and extraction of lithium ions, but also buffer the volume change of Fe_2O_3 anodes during cycling[36,37]. Compared to the particle-on-sheet composite, the sheet-on-sheet composite showed better cycling performances. The Fe_2O_3-graphene sheet-on-sheet has a high reversible charge capacity of 800.6 mAh g^{-1} after 50 cycles, which is almost 1.65 times as large as that of Fe_2O_3-graphene

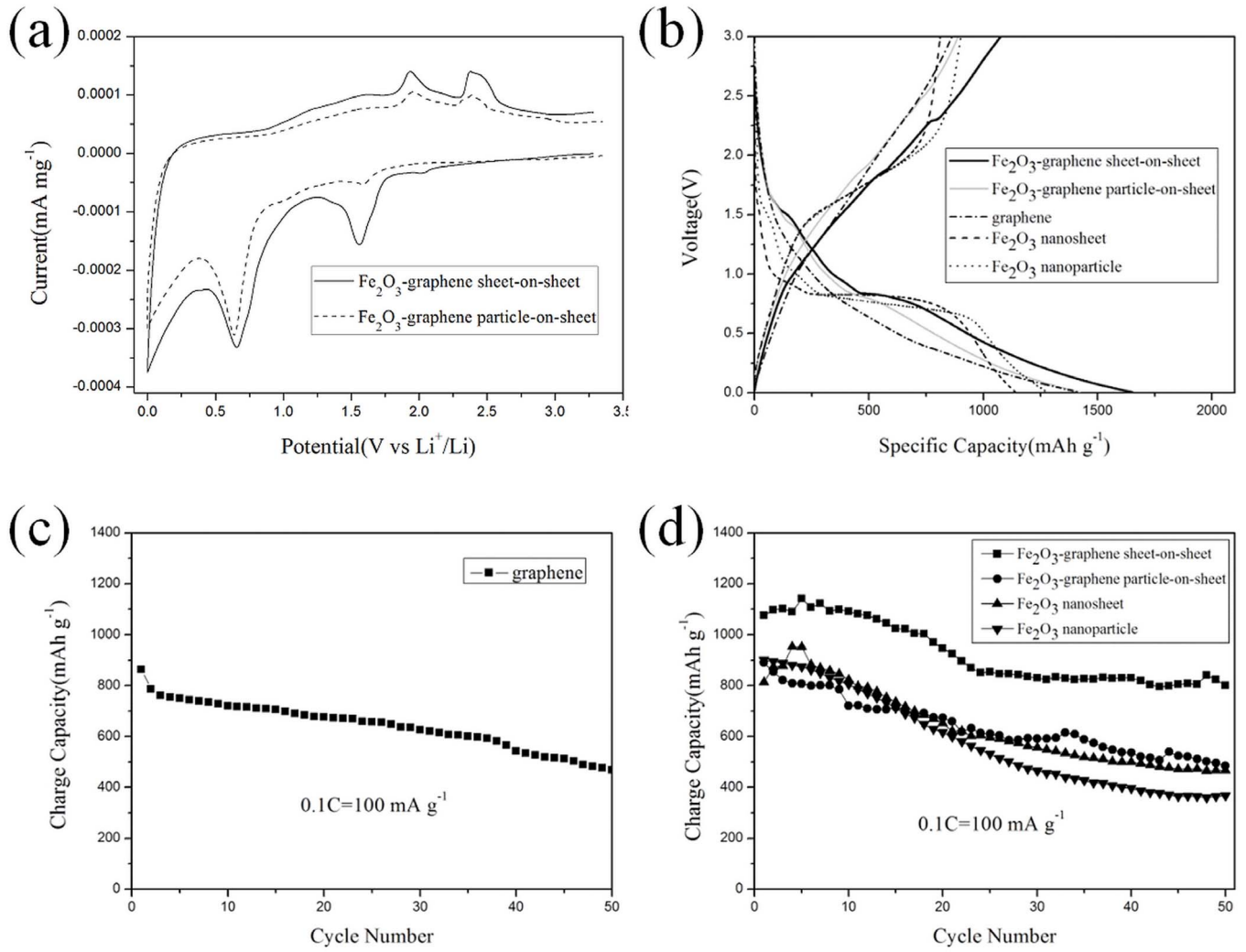

Figure 6 | Electrochemical lithium storage performances of Fe_2O_3-based at a low rate. (a) Cyclic voltammograms of Fe_2O_3-graphene composites at a scan rate of 0.1 mV s^{-1}, (b) First-cycle discharge (lithium insertion) and charge (lithium extraction) curves of various anodes, Cycling performances of (c) bare graphene, and (d) Fe_2O_3 based electrodes at 0.1 C.

particle-on-sheet (485.2 mAh g^{-1}) after the same cycle number. It is noted that the graphene content in Fe_2O_3-graphene sheet-on-sheet composite (59.4 wt%) is comparable to that of the particle-on-sheet composite (54.9 wt%) as indicated by TGA results.

The electrical conductivities of the obtained Fe_2O_3-based products were measured by a four-electrode method. Fe_2O_3 is highly insulated because its electrical conductivity is too small to be measured. In comparison, the electrical conductivities of Fe_2O_3-graphene composites are greatly enhanced and 0.156 S cm^{-1} and 0.138 S cm^{-1} were determined for the Fe_2O_3-graphene sheet-on-sheet and Fe_2O_3-graphene particle-on-sheet respectively. Due to the increased electrical conductivity, it is meaningful to explore the rate performances of Fe_2O_3-graphene composites. As shown in Fig. 7a–b, the Fe_2O_3-graphene sheet-on-sheet also exhibited an excellent rate capability. High initial charge capacities of 833.9, 798.6 and 792.2 mAh g^{-1} were observed at high current rates of 1, 2 and 5 C, respectively. After comparatively fast capacity fading in the first few cycles, the sheet-on-sheet composite showed a very stable cycliability in the following cycles. High capacities of 662.4, 456.2, and 322.5 mAh g^{-1} are retained after 100 cycles at 1, 2, and 5 C, respectively. Fig. 7c shows the high-rate cycling performances of Fe_2O_3-graphene particle-on-sheet composite. After 100 cycles of discharge and charge, reversible capacities of 318.1, 170.4, and 138.4 mAh g^{-1} were observed at 1, 2, and 5 C, respectively.

Discussion

These high-rate cycling performances of Fe_2O_3-graphene particle-on-sheet are much worse than those of Fe_2O_3-graphene sheet-on-sheet. Because two composites have similar values of electrical conductivities and comparable graphene contents in the composites, the observed large difference between the high-rate performances of two composites should be largely ascribed to their structure difference. Fe_2O_3 nanosheet has a better structure affinity with graphene compared to Fe_2O_3 nanoparticles. Therefore the agglomeration of graphene is prevented better in sheet-on-sheet structure compared to particle-on-sheet structure as confirmed by the BET measurements in Fig. 1c–d. Compared with graphene-supported Fe_2O_3 nanorice anode tested under similar test conditions[29], the Fe_2O_3-graphene sheet-on-sheet composite also reveals enhanced Li^+ storage properties especially at high current rates. For example, a charge capacity of 582 mAh g^{-1} was reported at 1 C after 100 cycles for graphene-supported Fe_2O_3 nanorice composite[29], however a higher charge capacity of 662.4 mAh g^{-1} was observed for the sheet-on-sheet composite in this work. It may be ascribed to the following points. The sheet-on-sheet composite should display the best structure affinity in all graphene-supported metal oxide morphologies because there are large intimate contact areas between these two types of two dimensional materials (Fe_2O_3 nanosheets and graphene nanosheets). Graphene nanosheets are separated well by numerous Fe_2O_3

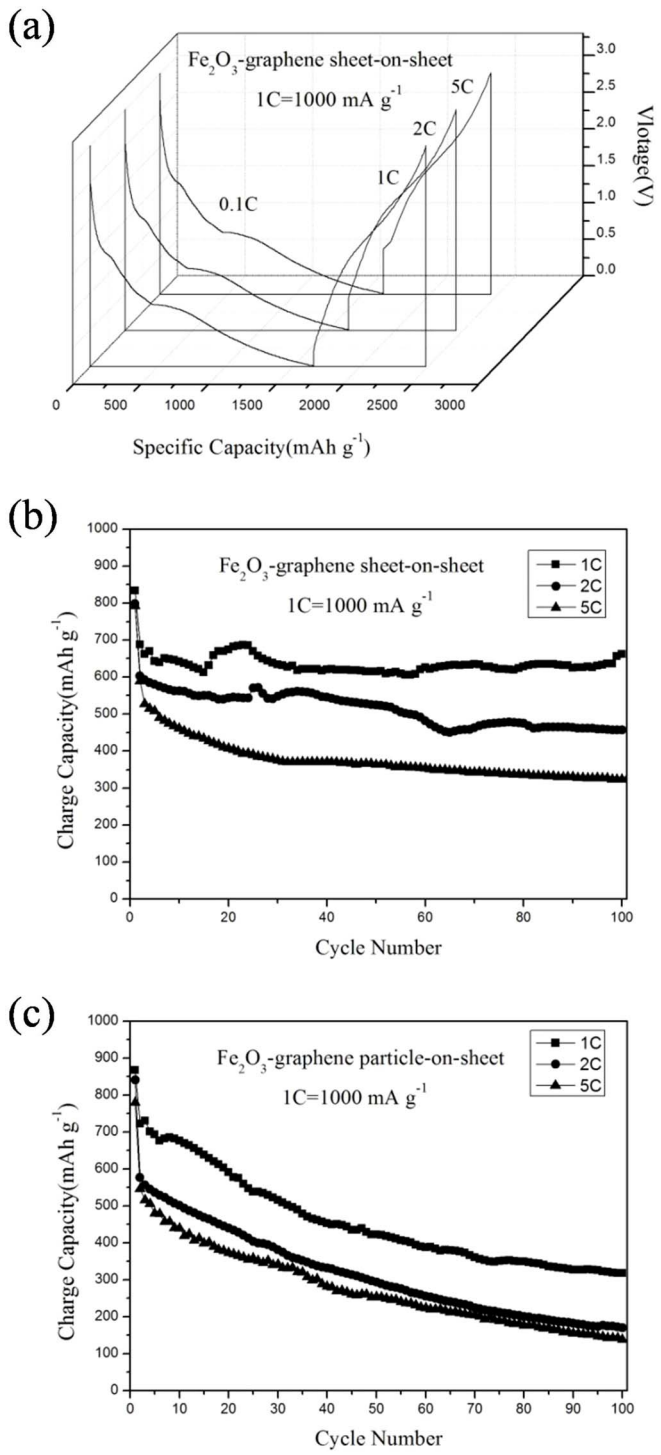

Figure 7 | Electrochemical lithium storage performances of Fe_2O_3-graphene composites at high rates. (a) First-cycle discharge (lithium insertion) and charge (lithium extraction) curves of Fe_2O_3-graphene sheet-on-sheet composite at large current rates, (b) High-rate cycling performances of Fe_2O_3-graphene sheet-on-sheet composite, and (c) High-rate cycling performances of Fe_2O_3-graphene particle-on-sheet composite.

nanosheets, thus reducing their chance of being agglomerated to form graphite platelets. This heavy agglomeration can destroy unique intrinsic promising properties of graphene nanosheet relative to their few-layer thickness nanostructure. Moreover, owing to the unique sheet-on-sheet nanostructure, graphene can buffer the volume change of Fe_2O_3 nanosheet anode due to Li^+ insertion/extraction reactions and increase their electrical conductivity and structure stability during repetitive cycling[36,37]. The AC impedance spectra measurements were also carried out to investigate the kinetics of electrode process. As shown in the Nyquist plots in Fig. 8a, the semicircles in the medium frequency is corresponded to the charge-transfer resistance (R_{ct}). It is clear that the R_{ct} value can be substantially decreased for those anodes in the presence of graphene. The diameter of the semicircle for Fe_2O_3-graphene sheet-on-sheet composite is also slightly shorter than that of the Fe_2O_3-graphene particle-on-sheet composite. Based on the equivalent circuit (Fig. 8b), the R_{ct} of Fe_2O_3-graphene sheet-on-sheet, Fe_2O_3-graphene particle-on-sheet, Fe_2O_3 nanosheet, Fe_2O_3 nanoparticle were calculated to be 27.1, 34.8, 198.0, 210.7 Ω, respectively. These results are also supportive for superior high-rate performances observed for Fe_2O_3-graphene sheet-on-sheet composite.

In summary, a new Fe_2O_3-graphene sheet-on-sheet composite was reported in this work. The growth mechanism of Fe_2O_3-based products with various morphologies and sizes was also explored. Compared to Fe_2O_3 nanoparticle, Fe_2O_3 nanosheet was found to be a better spacing structure to be composited with graphene nanosheets, which hinders the agglomeration of the latter. When used as an anode for Li-ion battery, the sheet-on-sheet nanostructure exhibited a high reversible capacity of 1074.9 mAh g^{-1} with good cycling performance at 0.1 C. This composite also exhibited an excellent high-rate capability. A high reversible capacity of 622.4 mAh g^{-1} was retained after 100 cycles at a high current rate of 1 C.

Methods

Preparation of graphite oxide (GO). Graphite oxide was synthesized from natural graphite by a modified Hummer's method[25,48]. 1 g natural graphite powder was mixed with 50 mL 65 wt% HNO_3 and 50 mL 98 wt% H_2SO_4 in an ice bath. After strong magnetic stirring for 30 min, 5 g $KMnO_4$ was added gradually and reacted for 2 h. 200 mL deionized water and 5 mL 30 wt% H_2O_2 were added dropwise to the mixture and the solution color changed to brilliant yellow, followed by washing with 15 ml 10 wt% HCl aqueous solution. The mixture was then centrifuged (12000 rpm) and washed with deionized water. Graphite oxides were obtained after drying on vacuum. After thermal reduction heating in a tube furnace in N_2 at 300°C for 2 h, the resultant black powders were collected as graphene nanosheets.

Preparation of Fe_2O_3-graphene composites. 0.027 g $FeCl_3.6H_2O$ and 0.08 g CH_3COONa were dissolved in 10 ml isopropanol with a trace amount of 0.07 mL deionized water. 0.016 g graphene nanosheets (GNS) were, also dispersed in 10 mL isopropanol and 0.07 mL deionized water by ultrasonication, and then mixed with previous $FeCl_3$ precursor solution (the theoretical weight ratio of Fe_2O_3 to GNS was 1 : 2). The mixture suspension was sealed in a 60 mL Teflon lined stainless steel autoclave and heated at 180°C for 12 h. After cooling to room temperature, the precipitate (Fe_2O_3-graphene sheet-on-sheet) was collected after copious washing by deionized water. The Fe_2O_3-graphene particle-on-sheet composite was prepared by the same method expect that 10 mL deionized water was used as the solvent to dissolve $FeCl_3$ and disperse GNS. Pristine Fe_2O_3 nanoparticles and nanosheets were also prepared by similar preparation process in the absence of GNS. Ethanol, propanol and isopropanol with various amounts of deionized water were also used to explore the solvent effect on the Fe_2O_3 products.

Materials characterizations. The obtained products were characterized by field-emission scanning electron microscopy (FE-SEM, JSM-6700F) with an energy dispersive X-ray spectrometer (EDS), transmission electron microscopy (TEM, JEOL JEM-200CX) and X-ray diffraction (XRD, Rigaku D/max-2550V, Cu Kα radiation). Raman spectroscopy was recorded on Renishaw in plus laser Raman spectrometer (excitation wavelength: 785 nm, excitation power: 3 mW, spot size: ~1.2 μm). The electrical conductivity was measured by a four-electrode method using a conductivity detection meter (Shanghai Fortune Instrument, FZ-2010). The specific surface area and porous structures were tested by an accelerated surface area and porosimetry analyzer (Micromeritics Instrument Corp, ASAP 2020 M + C, analysis adsorptive: N_2). Thermogravimetric analysis (TGA) was performed on a NETZSCH STA 409 PG/PC instrument in air.

Electrochemical measurements. The working electrodes were composed of 80 wt% of active material, 10 wt% of the conductivity agent (acetylene black), and 10 wt% of the binder (poly(vinylidene difluoride)), PVDF, Aldrich). The loading amount of the electrode on copper foil was kept at ~2 mg cm^{-2}. The thickness of electrode materials was ~20 micrometers. Lithium foil (China Energy Lithium) was used as counter and reference electrode. The electrolyte was 1 M $LiPF_6$ in a 50 : 50 w/w mixture of ethylene carbonate (EC) and diethyl carbonate (DEC). Electrochemical measurements were performed on a LAND-CT2001C test system. The Swagelok-type cells were discharged (lithium insertion) and charged (lithium extraction) at a constant current

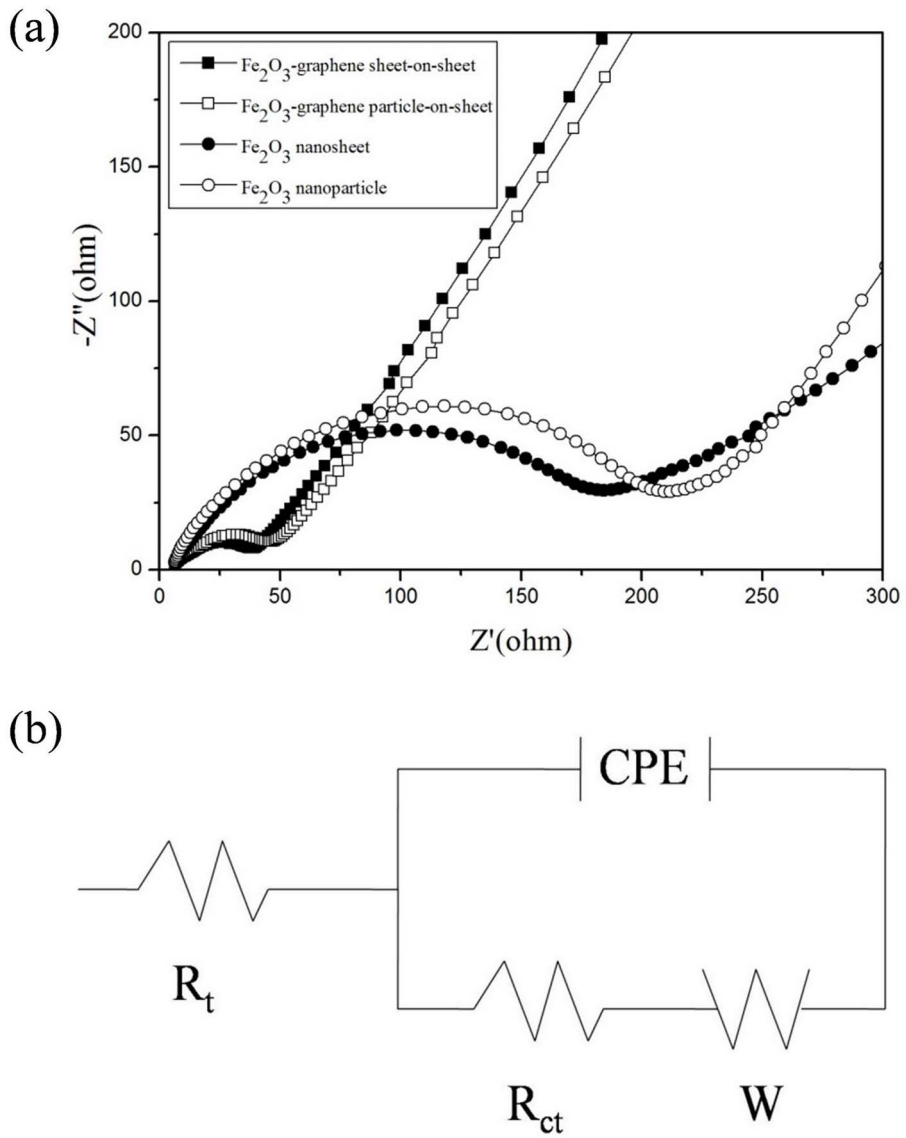

Figure 8 | Nyquist plots of Fe_2O_3-based electrodes. (a) Nyquist plots of Fe_2O_3-graphene sheet-on-sheet, Fe_2O_3-graphene particle-on-sheet, Fe_2O_3 nanosheet, Fe_2O_3 nanoparticle anodes, (b) Equivalent circuit for the electrode interface.

(100 mA g^{-1}, 0.1 C, 1 C = 1000 mA g^{-1}) in the fixed voltage range 5 mV to 3.0 V. Higher hourly rates (1, 2, or 5 C) were also used, and the first cycle discharging was kept at 0.1 C. Cyclic voltammetry (CV) was performed on a CHI660D electrochemical workstation at a scan rate of 0.1 mV s^{-1}. Nyquist plots were collected on the same workstation for various electrodes at a discharged potential of 0.8 V versus Li^+/Li after 5 cycles from 100 kHz to10 mHz.

1. Su, D. W., Ford, M. & Wang, G. X. Mesoporous NiO crystals with dominantly exposed {110} reactive facets for ultrafast lithium storage. *Sci. Rep.* **2**, 924 (2012).
2. Kaskhedikar, N. A. & Maier, J. Lithium Storage in Carbon Nanostructures. *Adv. Mater.* **21**, 2664–2680 (2009).
3. Cheng, F. Y., Liang, J., Tao, Z. L. & Chen, J. Functional Materials for Rechargeable Batteries. *Adv. Mater.* **23**, 1695–1715 (2011).
4. Kim, M. G. & Cho, J. Reversible and High-Capacity Nanostructured Electrode Materials for Li-Ion Batteries. *Adv. Funct. Mater.* **19**, 1497–1514 (2009).
5. Liu, X. J., Wang, H., Su, C. H., Zhang, P. W. & Bai, J. B. Controlled fabrication and characterization of microspherical $FeCO_3$ and α-Fe_2O_3. *J. Colloid Interface Sci.* **351**, 427–432 (2010).
6. Chen, L. Q. *et al.* Continuous Shape- and Spectroscopy-Tuning of Hematite Nanocrystals. *Inorg. Chem.* **49**, 8411–8420 (2010).
7. Morales, J., Sánchez, L., Martín, F., Berry, F. & Ren, X. L. Synthesis and characterization of nanometric iron and iron-titanium oxides by mechanical milling: Electrochemical properties as anodic materials in lithium cells. *J. Electrochem. Soc.* **152**, A1748–A1754 (2005).
8. Wu, X. L., Guo, Y. G., Wan, L. J. & Hu, C. W. α-Fe_2O_3 Nanostructures: Inorganic Salt-Controlled Synthesis and Their Electrochemical Performance toward Lithium Storage. *J. Phys. Chem. C* **112**, 16824–16829 (2008).
9. NuLi, Y., Zeng, R., Zhang, P., Guo, Z. P. & Liu, H. K. Controlled synthesis of α-Fe_2O_3 nanostructures and their size-dependent electrochemical properties for lithium-ion batteries. *J. Power Sources* **184**, 456–461 (2008).
10. Ma, J. M., Lian, J. B., Duan, X. C., Liu, X. D. & Zheng, W. J. α-Fe_2O_3: Hydrothermal Synthesis, Magnetic and Electrochemical Properties. *J. Phys. Chem. C* **114**, 10671–10676 (2010).
11. Chen, J., Xu, L. N., Li, W. Y. & Guo, X. L. α-Fe_2O_3 nanotubes in gas sensor and lithium-ion battery applications. *Adv. Mater.* **17**, 582–586 (2005).
12. Reddy, M. V. *et al.* α-Fe_2O_3 nanoflakes as an anode material for Li-ion batteries. *Adv. Funct. Mater.* **17**, 2792–2799 (2007).
13. Pan, Q. T. *et al.* Synthesis of α-Fe_2O_3 dendrites by a hydrothermal approach and their application in lithium-ion batteries. *J. Phys. D-Appl. Phys.* **42**, 015417 (2009).
14. Sun, B. *et al.* Synthesis of Mesoporous α-Fe_2O_3 Nanostructures for Highly Sensitive Gas Sensors and High Capacity Anode Materials in Lithium Ion Batteries. *J. Phys. Chem. C* **114**, 18753–18761 (2010).
15. Chen, J. S., Zhu, T., Yang, X. H., Yang, H. G. & Lou, X. W. Top-Down Fabrication of α-Fe_2O_3 Single-Crystal Nanodiscs and Microparticles with Tunable Porosity for Largely Improved Lithium Storage Properties. *J. Am. Chem. Soc.* **132**, 13162–13164 (2010).
16. Wang, H. L. *et al.* Mn_3O_4-Graphene Hybrid as a High-Capacity Anode Material for Lithium Ion Batteries. *J. Am. Chem. Soc.* **132**, 13978–13980 (2010).
17. Chou, S. L. *et al.* The compatibility of transition metal oxide/carbon composite anode and ionic liquid electrolyte for the lithium-ion battery. *J. Appl. Electrochem.* **41**, 1261–1267 (2011).

18. Hang, B. T., Watanabe, I., Doi, T., Okadab, S. & Yamaki, J. I. Electrochemical properties of nano-sized Fe_2O_3-loaded carbon as a lithium battery anode. *J. Power Sources* **161**, 1281–1287 (2006).
19. Hassan, M. F., Rahmana, M. M., Guo, Z. P., Chen, Z. X. & Liu, H. K. Solvent-assisted molten salt process: A new route to synthesise α-Fe_2O_3/C nanocomposite and its electrochemical performance in lithium-ion batteries. *Electrochim. Acta* **5**, 5006–5013 (2010).
20. Zhang, W. M. *et al.* Tin-nanoparticles encapsulated in elastic hollow carbon spheres for high-performance anode material in lithium-ion batteries. *Adv. Mater.* **20**, 1160–1165 (2008).
21. Gu, Y., Wu, F. D. & Wang, Y. Confined Volume Change in Sn-Co-C Ternary Tube-in-Tube Composites for High-Capacity and Long-Life Lithium Storage. *Adv. Funct. Mater.* **23**, 893–899 (2013).
22. Novoselov, K. S. *et al.* Electric field effect in atomically thin carbon films. *Science* **306**, 666–669 (2004).
23. Guo, P., Song, H. H. & Chen, X. H. Electrochemical performance of graphene nanosheets as anode material for lithium-ion batteries. *Electrochem. Commun.* **11**, 1320–1324 (2009).
24. Wang, C. Y., Li, D., Too, C. O. & Wallace, G. G. Electrochemical Properties of Graphene Paper Electrodes Used in Lithium Batteries. *Chem. Mater.* **21**, 2604–2606 (2009).
25. Zou, Y. Q. & Wang, Y. NiO nanosheets grown on graphene nanosheets as superior anode materials for Li-ion batteries. *Nanoscale* **3**, 2615–2620 (2011).
26. Lu, L. Q. & Wang, Y. Sheet-like and fusiform CuO nanostructures grown on graphene by rapid microwave heating for high Li-ion storage capacities. *J. Mater. Chem.* **21**, 17916–17921 (2011).
27. Chen, S. Q. & Wang, Y. Microwave-assisted synthesis of a Co_3O_4-graphene sheet-on-sheet nanocomposite as a superior anode material for Li-ion batteries. *J. Mater. Chem.* **20**, 9735–9739 (2010).
28. Gu, Y., Xu, Y. & Wang, Y. Graphene-Wrapped CoS Nanoparticles for High-Capacity Lithium-Ion Storage. *ACS Appl. Mater. Inter.* **5**, 801–806 (2013).
29. Zou, Y. Q., Kan, J. & Wang, Y. Fe_2O_3-Graphene Rice-on-Sheet Nanocomposite for High and Fast Lithium Ion Storage. *J. Phys. Chem. C* **115**, 20747–20753 (2011).
30. Bai, S., Chen, S. Q., Shen, X. P., Zhua, G. X. & Wang, G. X. Nanocomposites of hematite (α-Fe_2O_3) nanospindles with crumpled reduced graphene oxide nanosheets as high-performance anode material for lithium-ion batteries. *RSC Adv.* **2**, 10977–10984 (2012).
31. Xiao, W. *et al.* Fe_2O_3 particles enwrapped by graphene with excellent cyclability and rate capability as anode materials for lithium ion batteries. *Appl. Surf. Sci.* **266**, 148–154 (2013).
32. Zhu, X. J., Zhu, Y. W., Murali, S. T., Stoller, M. D. & Ruoff, R. S. Nanostructured Reduced Graphene Oxide/Fe_2O_3 Composite As a High-Performance Anode Material for Lithium Ion Batteries. *ACS Nano* **5**, 3333–3338 (2011).
33. Xiao, L. *et al.* Self-Assembled Fe_2O_3/Graphene Aerogel with High Lithium Storage Performance. *ACS Appl. Mater. Inter.* **5**, 3764–3769 (2013).
34. Xue, X. Y., Ma, C. H., Cui, C. X. & Xing, L. L. High lithium storage performance of α-Fe_2O_3/graphene nanocomposites as lithium-ion battery anodes. *Solid State Sci.* **13**, 1526–1530 (2011).
35. Liu, S. Y. *et al.* Graphene Anchored with Nanocrystal Fe_2O_3 with Improved Electrochemical Li-Storage Properties. *Int. J. Electrochem. Sc.* **7**, 354–362 (2012).
36. Zhang, M. *et al.* A green and fast strategy for the scalable synthesis of Fe_2O_3/graphene with significantly enhanced Li-ion storage properties. *J. Mater. Chem.* **22**, 3868–3974 (2012).
37. Chen, D. Z., Wei, W., Wang, R. N., Zhu, J. C. & Guo, L. α-Fe_2O_3 nanoparticles anchored on graphene with 3D quasi-laminated architecture: in situ wet chemistry synthesis and enhanced electrochemical performance for lithium ion batteries. *New J. Chem.* **36**, 1589–1595 (2012).
38. Zhu, J. X. *et al.* Facile synthesis of metal oxide/reduced graphene oxide hybrids with high lithium storage capacity and stable cyclability. *Nanoscale* **3**, 1084–1089 (2011).
39. Tian, L. L. *et al.* The production of self-assembled Fe_2O_3-graphene hybrid materials by a hydrothermal process for improved Li-cycling. *Electrochim. Acta* **65**, 153–158 (2012).
40. Zhang, W. Y., Zeng, Y., Xiao, N., Hng, H. H. & Yan, Q. Y. One-step electrochemical preparation of graphene-based heterostructures for Li storage. *J. Mater. Chem.* **22**, 8455–8461 (2012).
41. Zhou, G. W. *et al.* Facile Spray Drying Route for the Three-Dimensional Graphene-Encapsulated Fe_2O_3 Nanoparticles for Lithium Ion Battery Anodes. *Ind. Eng. Chem. Res.* **52**, 1197–1204 (2013).
42. Du, M., Xu, C. H., Sun, J. & Gao, L. Synthesis of α-Fe_2O_3 nanoparticles from $Fe(OH)_{(3)}$ sol and their composite with reduced graphene oxide for lithium ion batteries. *J. Mater. Chem. A* **1**, 7154–7158 (2013).
43. Qu, J. *et al.* Layer Structured α-Fe_2O_3 Nanodisk/Reduced Graphene Oxide Composites as High-Performance Anode Materials for Lithium-Ion Batteries. *ACS Appl. Mater. Inter.* **5**, 3932–3936 (2013).
44. Zhang, C. M. *et al.* Synthesis of hexagonal-symmetry α-iron oxyhydroxide crystals using reduced graphene oxide as a surfactant and their Li storage properties. *CrystEngComm* **14**, 147–153 (2012).
45. Lu, L. Q. & Wang, Y. Facile synthesis of graphene-supported shuttle-and urchin-like CuO for high and fast Li-ion storage. *Electrochem. Commun.* **14**, 82–85 (2012).
46. Yang, S. B. *et al.* Porous Iron Oxide Ribbons Grown on Graphene for High-Performance Lithium Storage. *Sci. Rep.* **2**, 427 (2012).
47. Tuinstra, F. & Koenig, J. L. Raman Spectrum of Graphite. *J. Chem. Phys.* **53**, 1126–1130 (1970).
48. Hummer, W. S. & Offeman, R. E. Preparation of Graphitic Oxide. *J. Am. Chem. Soc.* **80**, 1339 (1958).

Acknowledgments

The authors gratefully acknowledge the financial support from the follow-up Program for Professor of Special Appointment (Eastern Scholar) in Shanghai, National Natural Science Foundation of China (51271105) and Shanghai Municipal Government (11JC1403900, 11SG38, S30109).

Author contributions

J.K. performed the experiments. J.K. and Y.W. designed the experiments, discussed the results and wrote the manuscript.

Additional information

Competing financial interests: The authors declare no competing financial interests.

How to cite this article: Kan, J. & Wang, Y. Large and fast reversible Li-ion storages in Fe_2O_3-graphene sheet-on-sheet sandwich-like nanocomposites. *Sci. Rep.* **3**, 3502; DOI:10.1038/srep03502 (2013).